ACS APPLIED MATERIALS & INTERFACES

www.acsami.org Research Article

Following in Situ the Degradation of Mesoporous Silica in Biorelevant Conditions: At Last, a Good Comprehension of the Structure Influence

Elisa Bindini, Zeinab Chehadi, Marco Faustini, Pierre-Antoine Albouy, David Grosso, Andrea Cattoni, Corinne Chanéac, Omar Azzaroni, Clément Sanchez, and Cédric Boissière*

Cite This: *ACS Appl. Mater. Interfaces* 2020, 12, 13598–13612 Read Online

ACCESS | Metrics & More | Article Recommendations | Supporting Information

ABSTRACT: Mesoporous silica nanoparticles (MSNs) have seen a fast development as drug delivery carriers thanks to their tunable porosity and high loading capacity. The employ of MSNs in biomedical applications requires a good understanding of their degradation behavior both to control drug release and to assess possible toxicity issues on human health. In this work, we study mesoporous silica degradation in biologically relevant conditions through in situ ellipsometry on model mesoporous nanoparticle or continuous thin films, in buffer solution and in media containing proteins. In order to shed light on the structure/dissolution relationship, we performed dissolution experiments far from soluble silicate species saturation. Via a complete decorrelation of dissolution and diffusion contributions, we proved unambiguously that surface area of silica vectors is the main parameter influencing dissolution kinetics, while thermal treatment and open mesoporous network architecture have a minor impact. As a logical consequence of our dissolution model, we proved that the dissolution lag-time can be promoted by selective blocking of the mesopores that limits the access to the mesoporous internal surface. This study was broadened by studying the impact of the organosilanes in the silica structure, of the presence of residual structuring agents, and of the chemical composition of the dissolution medium. The presence of albumin at blood concentration was found affecting drastically the dissolution kinetics of the mesoporous structure, acting as a diffusion barrier. Globally, we could identify the main factors affecting mesoporous silica materials degradation and proved that we can tune their structure and composition for adjusting dissolution kinetics in order to achieve efficient drug delivery.

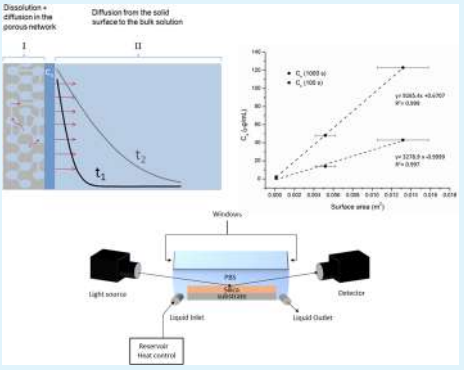

KEYWORDS: *therapeutic vectors, mesoporous silica, dissolution kinetic, ellipsometry, protein*

INTRODUCTION

In the field of nanomedicine, research on therapeutic vectors for drug delivery led to many synthesis strategies aiming at creating functional nanovectors with various properties. Three of them are mandatory for a successful application: (i) the targeting ability (usually for a tumor or a given organ), (ii) the ability to deliver drug in a controlled manner, and (iii) the ability to be cleared via nontoxic pathways (usually by biological degradation such as enzymatic lysis or by dissolution). From a pharmacokinetic point of view, an optimal effect is obtained when these three properties happen sequentially. So far, materials scientists have spent much effort on designing efficient nanovector architectures and delivery strategies, and very little literature can be found on the study of the in vivo fate of the carrier after drug release. The risk associated with uncontrolled degradation is either a non-targeted drug delivery or the in vivo accumulation of NPs leading to a limitation of administration frequency and/or toxic side effects. Yet, degradation studies in vivo are indeed very difficult to perform and require complex analytical approaches for recovering nanovectors from living tissues and/or the ability to analyze and discriminate within an organ between nanovectors and nanovector degradation products. From a physicochemical point of view, one key parameter to master is the control of nanoparticle degradation kinetics in the various environments in which vectors circulate (blood, extracellular matrix, endosomes, etc.). Consequently, much effort is still needed for creating nanovector architectures and compositions allowing a controlled degradation kinetic of the carrier concomitant with or following the drug release.

Received: November 12, 2019
Accepted: February 20, 2020
Published: February 20, 2020

https://dx.doi.org/10.1021/acsami.9b19956
ACS Appl. Mater. Interfaces 2020, 12, 13598–13612

In this aspect, mesoporous silica nanocarriers (MSNs) have attracted considerable attention as drug delivery nanocarriers.[1,2] Thanks to its excellent biocompatibility and high loading capacity, mesoporous silica is frequently employed to realize nanoparticles for drug delivery or in combination with other materials to form multifunctional core−shell structures.[3−6] Additionally, mesoporous silica materials provide easy functionalization with silane agents and adjustable pore sizes to host a very large amount of active molecules. As for other nanovectors, their use for biomedical applications raises the need to address their dissolution kinetics in vivo.

Silica is not chemically stable in water media as it undergoes hydrolysis forming orthosilicic acid and silicate oligomers. The hydrolysis of Si−O−Si bonds is the rate-limiting step of the reaction. The driving force of dissolution is the undersaturation in silicates of the medium at the vicinity of the vector's surface. As soon as saturation is reached (usually in confined media), silica can randomly nucleate and reprecipitate, getting to an equilibrium that hinders the complete dissolution of solid silica particles.[7] Besides, with its own porous architecture, this behavior can lead to random mesopore occlusion due to precipitation, further inhibiting dissolution by reduction of the accessible reactive surface.[8] The direct consequence of this aspect is that we must distinguish dissolution rates in a medium that reaches saturation and dissolution rates far from saturation conditions. If in the first case degradation can last several days (and eventually never be completed), in an undersaturated medium, mesoporous silica is degraded within a few hours.[7,9−11] Thus, for better control of the silica dissolution rate, as well as to obtain unhindered drug release, it is more appropriate to perform experiments well below saturation limits, in conditions known as "sink conditions".

Silica solubility strongly depends also on two main classes of parameters: on its composition and on the properties of surrounding media. The degradation of mesoporous silica particles and films under physiological conditions has been studied in vitro using simulated body fluids, physiological buffers, and biological media[7,9−19] finding dissolution rates going from several hours to several days depending on the experimental conditions and silica structure.

Silica bulk composition influences dissolution kinetics and so does the material structure since the Si−O bond length and energy vary in different silica materials causing hydrolysis to happen at different rates.[20] Introducing heteroatoms such as Zr or Al results in an effective way to increase silica hydrolytic stability,[7,10] and grafting the silica surface with polymers or ligands also alters its dissolution kinetics.[13,21] Moreover, the structural organization of silica at a small scale can influence its surface reactivity, as discovered by Zhang et al.,[22] and, consequently, its dissolution rate. Different methods of synthesis can produce silicas with different bulk structures (e.g., the presence or absence of strained cyclic species or predominance of highly connected species[23]) that do not react with the same kinetics. This could explain some of the conflicting data found in the literature about silica dissolution kinetics. The surrounding medium characteristics strongly influence the dissolution rate as well; in particular, temperature and pH are known to be important parameters to tune silica solubility, which starts to increase abruptly above pH 9[24] and depends on temperature.[25] The presence of ions and molecules alters silica dissolution kinetics, for example, in the presence of Ca^{2+} and Mg^{2+} cations, and calcium/magnesium silicates are formed at the silica surface, protecting underneath silica from further dissolution.[9] Icenhower and Dove showed that the presence of NaCl in the solution can also increase dissolution rates up to a factor of 20.[20] When silica NPs are engineered with surface ligands or polymers, the interactions with molecules or ions in the surrounding medium can differ sensibly with respect to bare silica NPs, leading to important changes in dissolution rates. Overall, although understanding silica degradation is a decisive step toward its use in drug delivery, existing reports on silica stability are inconsistent and very difficult to compare for environmental conditions and vector concentration, size, and architecture differ a lot from one study to another. As a consequence, it is very difficult to address and rationalize the structure/dissolution kinetics relationship of such a type of nanocarrier.

In this work, we present a normalized approach aiming at determining the relationship between MSN structural parameters and their dissolution kinetics at pH 7.4 and a temperature of 37 °C. In order to predict MSN behavior in the bloodstream, undersaturated environments were tested. Undersaturation allows observation of the material evolution free from the saturation effect, which slows down and eventually avoids complete dissolution. We aimed to compare the influence of some main regulating factors that control mesoporous silica degradation in biorelevant conditions, varying them one at a time, to identify the ones having the biggest impact on the degradation kinetics. The recently developed analytical approach used is based on in situ ellipsometric analysis of mesoporous thin films having a thickness similar to the diameter of a MSN.[7,10] Such a strategy has the advantage over NPs to expose a plane interface, allowing ellipsometric analysis with a good time resolution of a few seconds.[26] With this method, structural evolutions of the silica-based nanostructure (porous volume, size) can be monitored during the degradation process, leading to a better understanding of the overall behavior (in contrary to NP studies where dissolution kinetics are usually evaluated through silica titration, losing most of the information on the material structural changes). Between the main structural factors, we considered surface area, porosity, silica condensation degree, and porous network morphology. Here, we separated the contribution of these parameters, analyzing their influence on the overall degradation kinetics. We demonstrated that pore-blocking due to molecule adsorption can change the degradation kinetics, introducing a lag-time period, which is a very interesting behavior for drug carriers as discussed in this manuscript.

In parallel with this study, we compared the degradation kinetics of mesoporous silica and usual hybrid organosilica (known for increasing hydrolytic stability),[7,27,28] containing covalently linked aminopropyl moieties. We confirmed the role of organosilanes in slowing down the silica degradation, shedding some light on the degradation mechanisms of hybrid organosilica materials. We also addressed the influence of the degradation media and, particularly, of protein-rich media. Remarkably, we showed that mesoporous silica dissolution kinetics is strictly proportional to the accessible surface area while mesoporous structure ordering and thermal treatment do not play a major role. We also demonstrated that the surrounding media composition (in particular, the presence of proteins) can control silica degradation speed in biological media. Moreover, this case study is representative of the first, important stage of drug delivery: after injection in the

https://dx.doi.org/10.1021/acsami.9b19956
ACS Appl. Mater. Interfaces 2020, 12, 13598−13612

bloodstream, NPs are in an undersaturated medium until they are internalized by cells.

EXPERIMENTAL SECTION

Mesoporous Silica Thin-Film Synthesis and Characterization. Mesoporous thin films are synthesized with the evaporation induced self-assembly (EISA) approach, employing hexadecyltrimethylammonium bromide (CTAB) and Pluronic F127 as templating agents,[29] indicated with letters CT and F, respectively. Briefly, templating surfactants were dissolved in H_2O/EtOH/HCl together with inorganic precursors such as tetraethoxysilane (TEOS) and 3-aminopropyl triethoxysilane (APTES). They were added in determined proportions to obtain solutions described in Tables 1 (silica) and 2 (hybrid organosilica). Solutions were stirred for 72 h at room temperature. Resulting sols were coated on silicon substrates by dip-coating (ACEdip from SolGelWay, Paris, France) at withdrawal speed u = 2 mm s^{-1}, 26 °C, and 30−35% relative humidity (RH), obtaining film thicknesses of 100−150 nm. Thin films were then stabilized for 16 h at 130 °C. Surfactants were removed by extraction in ethanol (3 × 5 min). Some references of calcined silica films were treated 30 min at 200 °C and 10 min at 450 °C and are identified as CT450 when templated with CTAB and F450 when templated with Pluronic F-127.

Table 1. Molar Composition of Solution Used To Prepare Mesoporous Silica Thin Films Templated with CTAB Surfactant (CT Samples) and F-127 Surfactant (F Samples)

sample	TEOS	EtOH	HCl	H_2O	Pluronic F-127	CTAB
CT	1	40	0.09	5		0.14
F	1	40	0.09	5	0.005	

Table 2. Molar Composition of Solution Used To Prepare Hybrid Organosilica Mesoporous Thin Films

sample	APTES	TEOS	EtOH	HCl	H_2O	CTAB
NCT	0.15	0.85	40	0.24	5	0.14

Hybrid organosilica films (NCT) were obtained by co-condensation of TEOS and APTES and templated with CTAB; they have propyl-amine groups anchored to the silica matrix.

Nanoparticle (NP) Thin-Film Synthesis and Characterization. Mesoporous silica nanoparticles were synthesized adding 3 mL of a solution 0.88 M TEOS in EtOH to a solution of CTAB (0.29 g) in water (125 mL) and ammonia 0.512 M (25 mL). The water/ammonia solution was kept at 50 °C under stirring (750 rpm) during the addition of TEOS solution. The nucleation happened in the first 3 min at 50 °C, and the solution was then kept under stirring at r.t. for 2 h. The sol containing the silica particles was dip-coated on a silicon substrate at u = 0.01 mm s^{-1} and 50 °C to obtain a homogeneous layer of nanoparticles. The film was then heated at 130 °C for 16 h and washed in EtOH to remove CTAB (3 × 10 min). NPs and NP films were imaged by scanning electron microscopy (SEM) operated on a Hitachi SU-700.

GI-SAXS. The mesostructure of thin films was analyzed by grazing incidence small-angle X-ray scattering (GI-SAXS). Patterns were recorded on a homemade setup. It consists of a rotating anode generator (copper anode; small focus 0.1 × 0.1 mm^2, operated at 40 kV, 20 mA) equipped with a multilayer collimating optic. The sample was placed on a rotational stage and was allowed to oscillate by a few degrees at grazing incidence during data collection. The pattern was recorded on a photo-stimulable imaging plate, and a vacuum pipe was inserted between the sample and the detector to minimize air scattering. The sample-to-detector distance was 600 mm. Typical exposure time was 20′.

Spectroscopic Ellipsometry. Ellipsometry and environmental ellipsometric porosimetry (EEP) analyses were recorded with a UV-IR (193−1690 nm) variable-angle spectroscopic ellipsometer (VASE) M2000DI from Woollam. Ellipsometry measurements were performed at an incidence angle of 75°, and the data analysis was performed with the CompleteEASE software, modeling the deposited sol−gel layers with a Cauchy dispersion model. EEP analyses were performed to evaluate the accessible porous volume and pore size distribution of the mesostructured films, employing a controlled atmosphere cell in which relative humidity (RH) was set by mass flow controllers and varied from 0 to 100%.[30,31] A Bruggeman effective medium approximation (BEMA) model was used to obtain porosity values. Pore size distribution was calculated from water physisorption isotherms through a modified Kelvin equation at the relative humidity value of capillary condensation. Surface area values are obtained from EEP data using a t plot analysis as described in ref 26.

X-ray Photoelectron Spectroscopy (XPS). XPS experiments were performed on a spectrometer from Omicron Scienta. Kinetic energies of electrons were measured through an Argus hemispheric analyzer. The XPS analyses were carried out using a monochromatic K Al (α) source (1486.6 eV, 300 W). The instrument was calibrated to give a binding energy (BE) of 103.3 eV for the Si 2p corresponding to Si in SiO_2 samples. An electron gun (1 eV, 5 mA) was used on all specimens as a charge neutralizer system. Peak fitting of XPS spectra was performed with CasaXPS.

Dissolution in PBS. 10 mM (mmol L^{-1}) phosphate buffer was prepared from phosphate-buffered saline (PBS) tablets (Sigma-Aldrich) dissolved in MilliQ water. This buffer solution was used as a medium for dissolution experiments and the preparation of the protein solution. For silica degradation studies in PBS (pH 7.4), we employed a thermostatic liquid cell of 5 mL volume from Woollam. Experiments were performed at 37 °C in static media, collecting data every 60 s. We worked in nonsaturated conditions, with the silica mass involved in every experiment around 0.015 mg/mL, far below the silica saturation limit at 37 °C, which is 147 μg mL^{-1}.[25] The setup employed is represented in Figure 1. For dissolution, thin films were modeled with a two-component BEMA employing silica or hybrid organosilica as the first component and PBS as the second component (optical properties of inorganic matrix and PBS were previously measured by ellipsometry; the ones of silica were evaluated on a dense film of similar composition). The Bruggeman effective medium approximation (BEMA) model allows determination of the relative volumetric fractions f_a and f_b of two materials A and B of known dielectric constants ε_a and ε_b within a volume unit of measured dielectric constant ε:

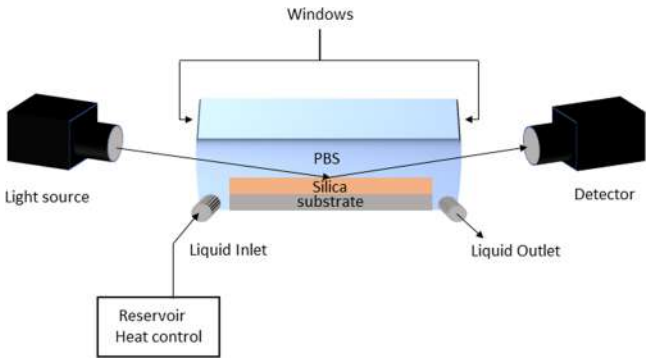

Figure 1. Experimental setup to investigate mesoporous silica thin-film degradation in PBS by in situ ellipsometry. Both the liquid cell and the liquid reservoir are kept to a constant temperature of 37 °C.

$$f_a \frac{\varepsilon_a - \varepsilon}{\varepsilon_a + 2\varepsilon} + f_b \frac{\varepsilon_b - \varepsilon}{\varepsilon_b + 2\varepsilon} = 0 \quad (1)$$

More details are given in the Supporting Information. With this method, we could calculate the volumetric fraction of silica f_s present

https://dx.doi.org/10.1021/acsami.9b19956
ACS Appl. Mater. Interfaces 2020, 12, 13598−13612

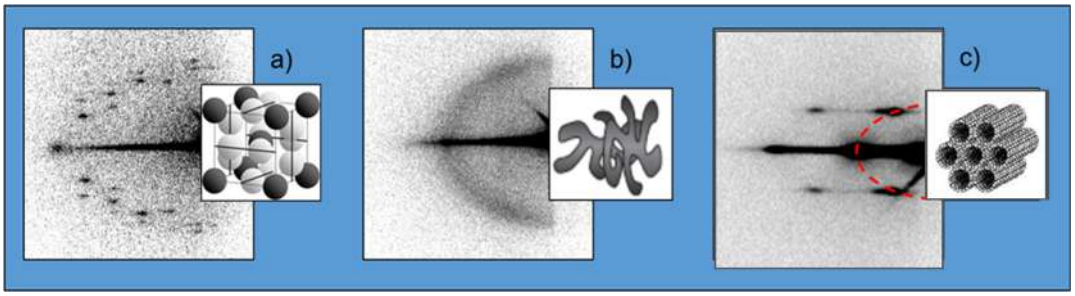

Figure 2. GI-SAXS patterns and the related mesostructures of mesoporous thin films obtained by dip-coating from solution at 26 °C and 30−35% RH: (a) silica templated with CTAB, *Pm3n* structure. (b) Hybrid organosilica templated with CTAB, wormlike structure. (c) Silica, templated with Pluronic F-127, *p6m* structure. More detail with the scale bar is provided in the Supporting Information.

Table 3. Structural Parameters of the Studied Mesoporous Silica Films[a]

sample	r_l (nm)	r_s (nm)	w_t (nm)	S (m^2 cm^{-3})	V_p (%)	structure	surfactant
CT130-1	1.6	1.5	1.2	700	45.5	*Pm3n*	CTAB
CT130-2				850	60.1	*Pm3n*	CTAB
CT130-3				650	42.0	*Pm3n*	CTAB
CT450-1	1.6	1.4	1.0	750	51.0	*Pm3n*	CTAB
CT450-2[b]	1.3	1.1		800	56.2	wormlike	CTAB
CT450-3	1.6	1.4	1.1	850	62.0	*Pm3n*	CTAB
CT450-4[c]				600	43.0	*Pm3n*	CTAB
CT450-5				600	43.1	*Pm3n*	CTAB
F450	2.9	2.0	5.7	370	61.4	*p6m*	Pluronic F-127
NCT130-1				600	42.0	wormlike	CTAB
NCT130-2				600	42.2	wormlike	CTAB

[a]Samples are identified with the templating surfactant (CT for CTAB and F for Pluronic F-127) and with the temperature at which they were stabilized (130 or 450 °C). We reported porous volume V_p and wall thickness w_t. Pore sizes were calculated assuming elliptical pores for *Pm3n* structures; semi-major axis (r_l) and semi-minor axis (r_s) of the ellipse are reported. For *p6m* and wormlike structures, a pore size distribution has been obtained assuming cylindrical pores with an elliptical base, where semi-axes are reported as semi-major axis (r_l) and semi-minor axis (r_s). [b]Just after the film deposition, the sample has been dried at relative humidity RH 75% and 37 °C for 20 min to obtain a wormlike mesostructure. [c]The sample was left 5 days on the laboratory bench before taking these data. Immediately after synthesis, it had a V_p of 61%.

in the film at every time point. Silica mass M was calculated from the silica volumetric fraction and the thickness of the film, assuming the walls to be chemically homogeneous with a density of amorphous silica fixed at 2.2 g cm^{-2}. For the hybrid organosilica film, we assumed a similar density. The dissolved silica mass M_t is then equal to the difference between initial mass M_0 and the silica fraction present in the film $M(t)$.

Dissolution in BSA Solution. To reproduce an environment mimicking more closely biological media, we performed dissolution experiments of mesoporous silica layers in a PBS solution of bovine serum albumin (BSA at 37 g L^{-1}, pH = 7.4). The chosen concentration was in the range of albumin concentration in human blood. In these conditions, BSA will be in its N form and exhibits an average negative surface charge.[57] Experiments were performed at 37 °C, employing the setup described in Figure 1 and the same protocol used for dissolution studies in PBS. The BSA solution remains transparent in the visible−NIR range, and it is thus possible to perform ellipsometry analysis "through" it.

Surface Plasmon Resonance (SPR). SPR experiments were performed on an SPR-Navi 210A from Bionavis, working at a fixed wavelength of 785 nm, in scanning angle mode. Analysis took place in two parallel channels of 1 μL of volume at 37 °C. Mesoporous silica was deposed by spin coating (4000 rpm, 30 s) on BK7 Glass slides (20 × 12 × 0.55 mm) coated with gold (SPR102-AU from Bionavis) and then cured at 130 °C overnight, obtaining a silica layer of 70 nm. CTAB was removed by washing with EtOH.

RESULTS AND DISCUSSION

Materials Characterizations. The mesostructuration of thin films obtained through EISA depends on several chemical and processing parameters and was characterized by grazing-incidence small-angle X-ray scattering.[32] Mesoporous silica films templated with CTAB have a *Pm3n* cubic structure, while films templated with Pluronic F-127 form a *p6m* 2D-hexagonal structure (Figure 2a,c). Hybrid organosilica films self-organize in wormlike structures (Figure 2b).

The pore volume V_p, specific surface area S, and pore size of mesoporous silica films were obtained from EEP data and are reported in Table 3 (isotherms are reported in the Supporting Information, Figure S2). Pore size was around 3 nm in diameter, and it was calculated assuming elliptical pores for *Pm3n* structures. The semi-major axis (r_l) and semi-minor axis (rs) of the ellipse are reported. For *p6m* and wormlike structures, a pore size distribution has been obtained assuming cylindrical pores with an elliptical base. From GI-SAXS experiments, the cell parameters of materials were obtained, and comparing them with pore sizes acquired through EEP, we calculated the silica wall thickness w_t.

Silica Dissolution in PBS, Theoretical Approach. Monitoring the degradation of mesoporous silica and hybrid organosilica thin films through in situ ellipsometry, we could assess the influence of some structural and exterior parameters on dissolution kinetics. We performed experiments in static undersaturated conditions at constant pH (7.4) and temperature (37 °C).

For describing the dissolution of a solid in a liquid, Noyes and Whitney elaborated an equation[33] in which dissolution is driven by the concentration gradient between the surface of

https://dx.doi.org/10.1021/acsami.9b19956
ACS Appl. Mater. Interfaces 2020, 12, 13598−13612

the solid material (where C_s is assumed to equal solubility at saturation of the solid) and concentration C in the bulk solution

$$\frac{\partial C}{\partial t} = k(C_s - C) \tag{2}$$

with $k = \frac{D}{Vh}$. Here, k is a constant factor gathering the diffusion coefficient of the dissolved species D, the volume of the solution V, and the width of the diffusion layer h. The concentration gradient is controlled by the diffusion process between the surface and the bulk solution. This model assumes that saturation is rapidly achieved at the solid−liquid interface (fast dissolution of the solid) and then diffusion takes place across a layer of stagnant solution, called diffusion layer, toward the bulk solution.[34] In the case of silica, which cannot be considered as a solid with fast dissolution kinetics, C_s will be assumed as the concentration of dissolved silica species at the external surface of the film where area is constant at 5 cm^2 (imposed by the liquid cell used for ellipsometry analysis). After integration, eq 3 gives the value of concentration of the solution at any given time $t \geq 0$:

$$C(t) = C_s(1 - e^{-kt}) \tag{3}$$

This model applies well in many cases of study where a dense solid dissolves in a liquid, and it has been adapted to several systems.[35−37] In that case, the concentration rise in solution is the factor limiting the dissolution kinetics.

Nevertheless, when the solid is mesoporous, other factors may influence its dissolution behavior. In fact, the dissolution process would take place in the mesopores, following first-order kinetics, and then the dissolved species would have to diffuse until the film interface with the bulk solution. From this point, we can assume that they will follow the Noyes−Whitney kinetics, but the overall dissolution kinetics has also to take into account the processes happening inside the porous network. This implies that C_s will not be rapidly equal to the solubility value, as assumed in the Noyes−Whitney model, but it will probably gradually increase toward this value, depending on both the dissolved amount and diffusion process inside the mesoporous structure. The dissolution process of a porous thin film can thus be divided into two phases: (i) dissolution and diffusion of the dissolved species from inside the porous network toward the film interface with the bulk solution and (ii) the diffusion of dissolved species from the interface to the bulk solution, following the Noyes−Whitney kinetics, driven by the concentration gradient and limited by saturation (Figure 3).

We performed dissolution experiments in a static environment, and in this case of figure, the diffusion layer thickness h is not constant, but it grows with $(Dt)^{1/2}$. The concentration profile due to diffusion of soluble species can be described with an erfc(t,x) function, where t is the diffusion time and x is the distance from the dissolution interface:

$$\frac{C(t, x)}{C_s} = \text{erf c}\left(\frac{x}{2\sqrt{Dt}}\right) \tag{4}$$

By reversing eq 4, we obtain the value of the diffusion layer thickness h, assuming that it is equivalent to a certain value of $x(t)$; for our calculations, we chose arbitrarily the value of $x(t)$ corresponding to a $C(x) = 0.1C_s$; that is, we assumed that the diffusion layer thickness is the distance at which the solution concentration is 10% of C_s. To do this inversion easily, we can

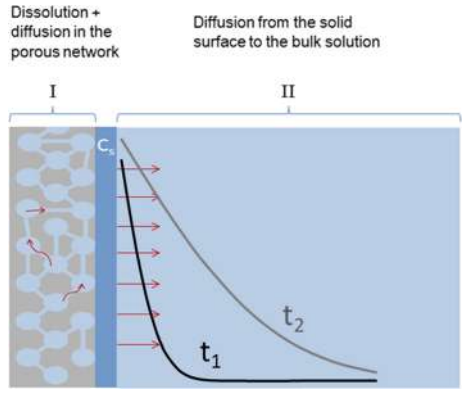

Figure 3. Scheme of the dissolution process of a mesoporous silica film with (red arrows) dissolved silicate species diffusion pathways, and black and gray curves are silicate diffusion layer concentration profiles represented at two different dissolution times t_1 and t_2.

approximate the erfc function as follows (comparison is shown in the Supporting Information):

$$\text{erf c}\,(x, t) = \exp\left[-1.9\left(\frac{x}{2\sqrt{Dt}}\right)^{1.3}\right] \tag{5}$$

obtaining eq 6 for $x(t)$ when $C(x)$ has reached 10% of the value of C_s.

$$x(t) = h(t) = 2.3186\sqrt{Dt} \tag{6}$$

Inserting eq 6 in eq 3, we can calculate the concentration C_s of dissolved silica at the external surface of the film as a function of time:

$$C_s(t) = \frac{C(t)}{\left[1 - \exp\left(-\frac{Dt}{Vh}\right)\right]} = \frac{C(t)}{\left[1 - \exp\left(-\frac{\sqrt{Dt}}{2.3186\,V}\right)\right]} \tag{7}$$

The values of $C_s(t)$ and $C(t)$ are reported in Figure 4 normalized for 1 cm^2 of silica films templated with CTAB and with F-127, using values of 1 mL for the dissolution volume V and of 1.3×10^{-9} m^2 s^{-1} for the diffusion coefficient of silicic acid in water at 37 °C.

As it can be seen, upon dissolution, C_s increases gradually and never reaches the saturation value of 147 $\mu g\ mL^{-1}$. We can observe that the maximum value of C_s is reached at different times for the two silica films, which have the same porous volume (62%) but very different pore sizes and surface areas. We can infer that the architecture of the mesoporous material affects the concentration at the interface C_s more precisely that the maximum value of the concentration at the solid−liquid interface C_s is reached faster when the specific surface area of the film is higher. If we report C_s at two different times versus the exact mesoporous surface per film area unit (taking into account film thicknesses), we find a very good linear correlation reported in Figure 5. At that stage, the fact that CTAB template films and F127 templated films have different pore connectivities does not seem to affect the correlation.

If we look at the thickness profile of the mesoporous films during dissolution, we observe that a huge swelling of the films takes place when C_s gets close to its maximum value; after this time point, C_s decreases and dissolution is slowed down (Figure 6), showing that either the dissolved species production decreases and/or its diffusion through the layer is slowed down.

https://dx.doi.org/10.1021/acsami.9b19956
ACS Appl. Mater. Interfaces 2020, 12, 13598−13612

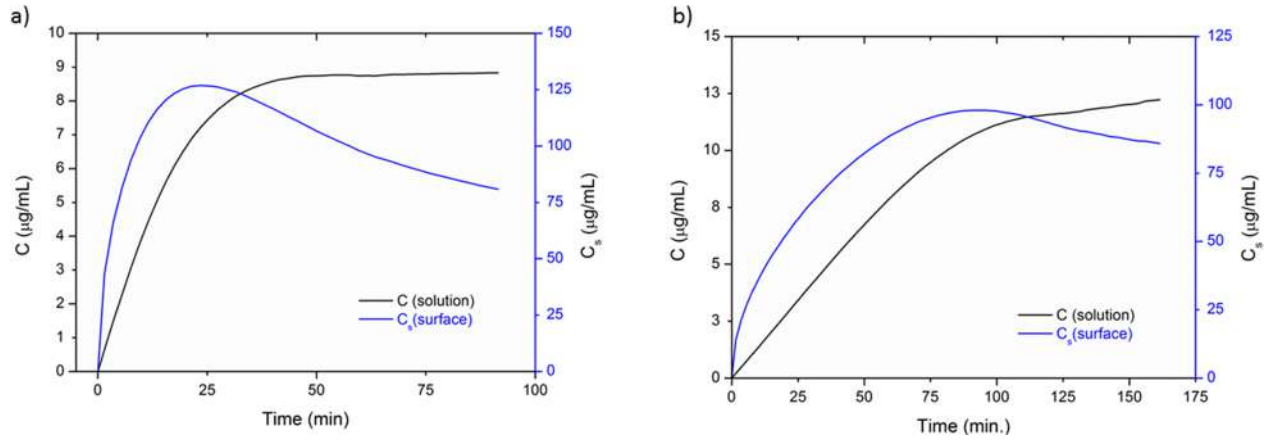

Figure 4. Bulk concentration (black line) and surface concentration (blue line) of dissolved silica for 1 cm^2 of mesoporous films having equivalent porous volume and template with (a) CTAB, sample CT450-3, and (b) Pluronic F-127, sample F450.

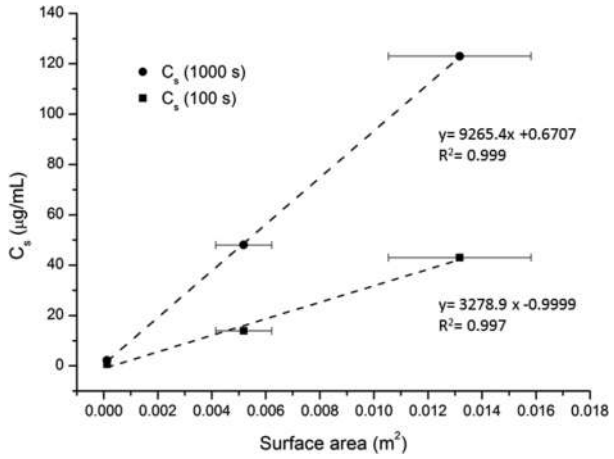

Figure 5. Concentration of dissolved silica at the solid−liquid interface after 100 (squares) and 1000 s (circles) is reported versus surface area of the mesoporous silica films. Linear fit is shown. The point at the lowest surface value refers to dense silica, while the porous samples have porosity values close to 62%. The surface area has been evaluated from EEP measurements with the *t* plot method. The error bars reported correspond to an error on the surface value of 20%.

We assume that such an effect is likely to be due to a solid to gel transformation of the layers, which is a documented behavior for siliceous materials.[38−42] If we extrapolate these results, the fact that the saturation concentration value is or is not reached by C_s depends very probably from the amount of silica in the film, suggesting that thick and thin films could behave differently and show different dissolution kinetics. Once the gel is formed, the diffusion of silicates species changes, affecting the dissolution kinetics of the material. For this reason, to compare the dissolution of different mesoporous silica thin films, we focused the following part of our work on the first part of the dissolution process before the material transformation in a swollen gel. This describes the silica dissolution of about 80 wt % of the material deposited. Such swelling is an unexpected behavior that, as far as we know, was never reported for the dissolution of mesoporous silica nanoparticles in simulated biological media. If one assumes that a similar swelling behavior takes place for nanoparticles, one has to keep in mind that films swell perpendicularly to the substrate only while nanoparticles would swell in 3D. As an example, 100% volume film swelling would mean a 26% increase of the NP radius. Yet this effect is only observed after more than 80% of silica is dissolved, which means that the objects in such a state exhibit a poor electronic density contrast, making them hard to spot for usual nanoparticle analysis techniques in the liquid state. This could explain why this effect has never been reported. Another possibility is that the rigid substrate of the film maintains the swollen gel in

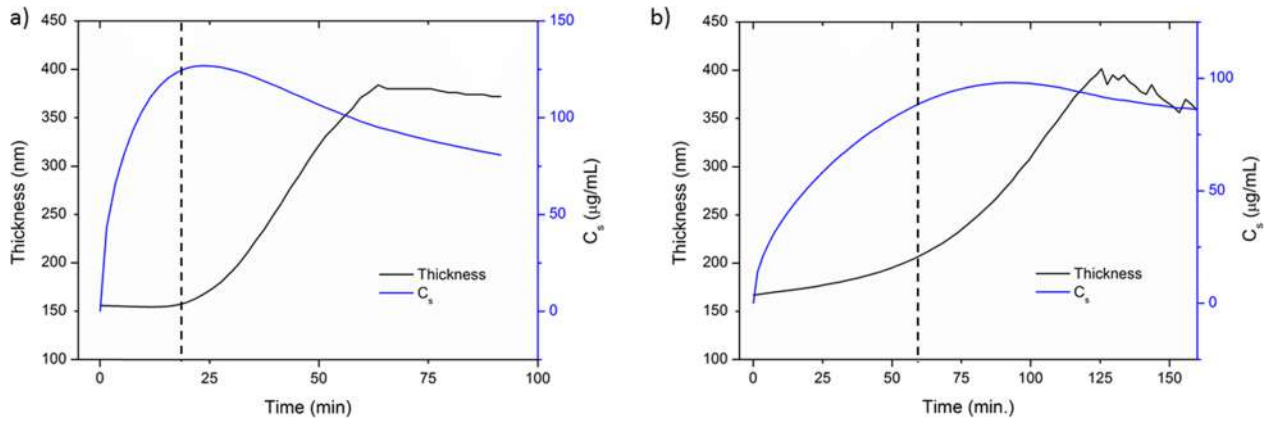

Figure 6. Thickness and C_s versus time for (a) mesoporous silica CT450-3 film and (b) mesoporous silica F450 film.

https://dx.doi.org/10.1021/acsami.9b19956
ACS Appl. Mater. Interfaces 2020, 12, 13598−13612

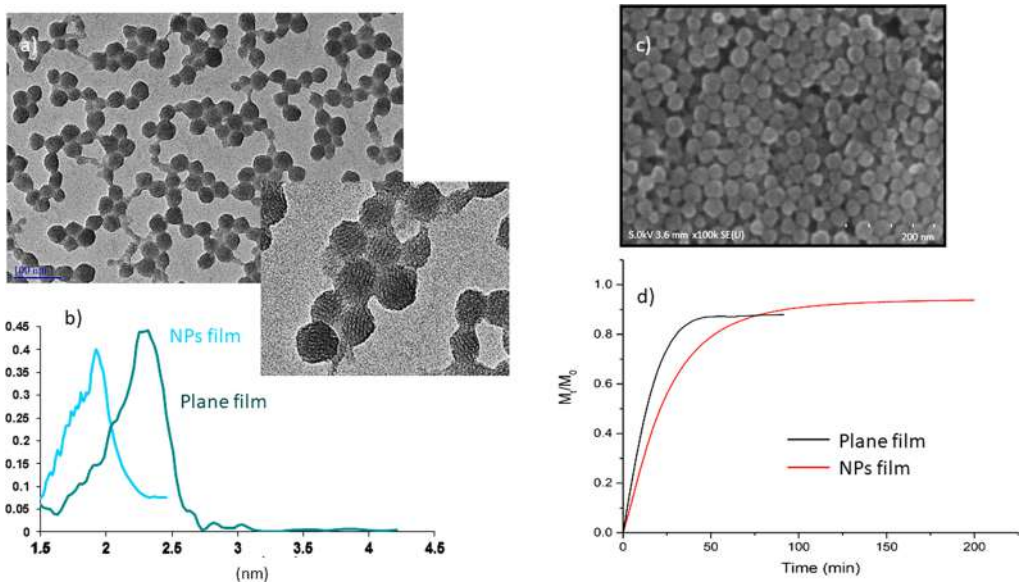

Figure 7. (a) TEM image of mesoporous silica nanoparticles templated with CTAB, particles have size of 40 nm and a *p6m* structure (see blow-up). (b) Pore size distribution of NP film and mesoporous silica plane film CT130-1, obtained from EEP measurements. (c) SEM image of NP film deposed on silicon. (d) Dissolution curves of NP film and plane film in PBS at 37 °C.

place, while with nanoparticles, it could shatter in smaller pieces.

To summarize these results, we learned that we can indeed separate the degradation process in two phases: (i) dissolution of silica and diffusion of the dissolved species through the porous network and (ii) diffusion from the external surface of the film toward the bulk solution. In the first part, the structure of the porous material affects dissolution kinetics, as already reported by Higuchi;[43] in that case, the diffusion can be considered limited by the accessible volume and network tortuosity. Higuchi described the diffusion in a porous solid by defining a diffusion coefficient $D_{eff} = DV_p/\tau$, where D is the diffusion coefficient when diffusion is not limited, V_p is the porous volume, and τ is the tortuosity. A full description of this part is limited by the lack of theory and normalized method for determining τ (which can be affected by mesopore size and connectivity). As we have seen above, in this phase, degradation kinetics is linearly correlated with the surface area. In the second phase, outside the porous film, dissolved species follow Fick's diffusion laws toward the bulk, driven by the concentration gradient, sticking to the Noyes–Whitney model.

Silica Dissolution in PBS, Normalized Approach. In order to compare more easily different samples degradation kinetics, the following part of this work will study dissolution kinetics by using the amount of dissolved silica M_t, normalized on starting silica mass M_0 as a function of dissolution time.

Continuous Films Versus Nanoparticle Films. As a first experiment, we verified the relevance of film models to explain nanoparticle degradation behavior. To do so, we compared the dissolution of a plane interface film of mesoporous silica and that of a film made of mesoporous silica NPs of similar mesostructure. For this experiment, we used mesoporous silica nanoparticles having diameters around 40 nm and 2D-hexagonal mesostructure (*p6m*) with pores of 2 nm. These have been prepared via usual silica-based therapeutic vector synthesis methods. Figure 7 shows images of NPs (Figure 7a) and of the multilayer film obtained by dip-coating the NP suspension on a silicon wafer (Figure 7c,d). The film refractive index at 632 nm was 1.102, meaning that the layer had a very high porosity, as expected for packed mesoporous nanoparticles. EEP data, reported in Figure S9, shows two adsorption steps, which correspond to the capillary condensation into the mesopores of the NPs (lower P/P_0) and to the filling of interparticle pores (higher P/P_0). Due to the interparticle porosity, huge surface roughness (≈45 nm from ellipsometric measurements), and a nonflat surface morphology, as can be seen from SEM image (Figure 7c), we could not calculate the total specific surface area with the *t* plot method using the film external surface area as reference (experimental and theoretical details are provided in ref 30.

These nanoparticles have usually surface areas ranging from 900 to 1100 $m^2\ g^{-1}$, but when packed in a multilayer film, they most probably lose some external surface area due to their compact spatial arrangement. Comparing the dissolution of a plane film and of a NP film having similar mesopore size distribution (Figure 7b), we observed similar degradation kinetics. The silica release for NP films is slower than for plain films. We estimated the surface area of the film made of NPs at 690 $m^2\ cm^{-3}$, assuming that NP compacity in the film is 60%, and their surface area is 1000 $m^2\ g^{-1}$. A comparison of dissolved amounts after 1000 s, normalized with the surface area of the samples, shows that both the NP-based film and continuous film have dissolution rates per square meter differing by only 18%. Even though we cannot rule out a different surface area evolution between a layer of nanoparticles and a plain layer (the former one having a higher external surface area than the latter), the very similar dissolution rate observed is encouraging. Yet, a comparison with experiments performed with suspended nanoparticles would be useful. One of the only articles working in similar concentration conditions (very far from saturation, same temperature and dissolution medium) is reported in ref 9. In this work, they observed that the complete dissolution of the mesoporous structure takes about 2 h (very close to our results). Both results obtained for deposited and suspended

https://dx.doi.org/10.1021/acsami.9b19956
ACS Appl. Mater. Interfaces 2020, 12, 13598−13612

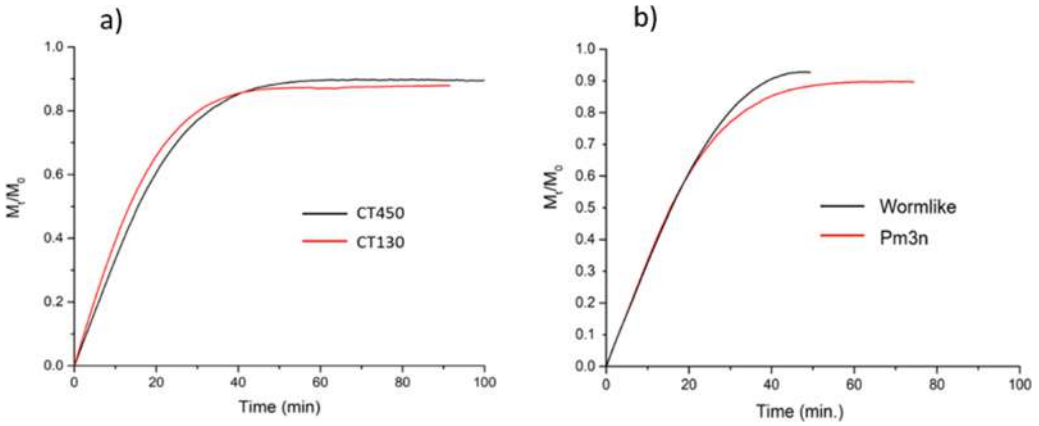

Figure 8. Dissolved silica mass M_t normalized on initial silica mass M_0 during dissolution in PBS at 37 °C of (a) mesoporous silica layers templated with CTAB and exposed to different thermal treatment (130 and 450 °C). Samples are CT130-2 (red line) and CT450-3 (black line). (b) Mesoporous silica layers templated with CTAB, heated at 450 °C, having different mesostructures; they have similar porosity (56% for the wormlike structure and 62% for the *Pm*3*n*) and surface area (800−850 m^2 cm^{-3}). Samples are CT450-2 (black line) and CT450-3 (red line).

nanoparticles strongly support the fact that kinetic dissolution data obtained with mesoporous films are relevant for studying the dissolution rate of mesoporous nanoparticles.

Effect of the Thermal Stabilization and the Meso-ordering of Silica Films. By comparing calcined and washed CTAB template mesoporous films, we observed that high-temperature thermal treatment does not improve silica stability toward hydrolysis to a great extent. In fact, dissolution curves of samples heated at 130 and 450 °C presenting similar surface area, mesostructure, and composition do not show much difference (Figure 8a). The dissolution of CT450 is only slightly slower than the one of CT130. This result is consistent with the fact that very little difference exists in the condensation degree of silica networks condensed with the HCl catalyst and treated at 150 and 450 °C (about 89% of Si−O−Si bonds are formed in both cases), as already reported[44] in a previous study.

To complete our structural investigation, we wanted to verify if the mesoporous structure can play a role in dissolution kinetics. To do so, we prepared CT450 samples under different relative humidity (RH) conditions during film deposition, to obtain a different arrangement of the mesopores, keeping constant all the other parameters.[29] We compared dissolution kinetics of samples having similar porosity (56−62%) and surface area values (800−850 m^2 cm^{-3}). We could observe that silica presenting a *Pm*3*n* cubic structure dissolves at the very same rate as silica having a wormlike structure for more than 70% of the dissolution process, that is, before the solid to gel transformation (Figure 8b), after which time we cannot argue any further about its structure. Thus, we can infer that the 3D organization of a mesoporous network does not significantly affect silica dissolution kinetics when other parameters are kept constant (mesopore size, porous volume, high pore connectivity). Anyway, it has to be mentioned that this is true for these kinds of structures having large porous volumes and many interconnections between mesopores, for which we can assume that diffusion is not particularly hindered. Analyzing porous networks less opened, the mesostructure could have a more important influence on diffusion and on the overall dissolution behavior.

Investigation of Pore-Blocking Effects. A classical problem met by experimentalists with mesoporous materials is that they exhibit high surface area and get quickly contaminated in air by volatile organic compounds (VOCs) or in solution by small soluble molecules that adsorb into the mesopores (see the Supporting Information, Figure S4). In such cases, when analyzed through EEP, their porous volume is reduced by a considerable amount, passing from 61−62% after the synthesis to 43% after 5 days of rest in a standard plastic box onto a laboratory bench (we assumed the refractive index of the adsorbed pollutant to be 1.45 at 700 nm). If the pores are blocked, not all the surface is available to react with water. Moreover, diffusion of the dissolved species may be hindered, slowing down the overall dissolution process. Indeed, performing dissolution experiments on these films, we noticed a slower dissolution rate and also a different shape of the dissolution curve, which becomes more sigmoidal (Figure 9). The reduced surface area and the hindered diffusion due to pore-blocking are likely to make dissolution kinetics slower at the beginning, but during the degradation process, adsorbates slowly diffuse out of the pores, leaving more surface available to react with

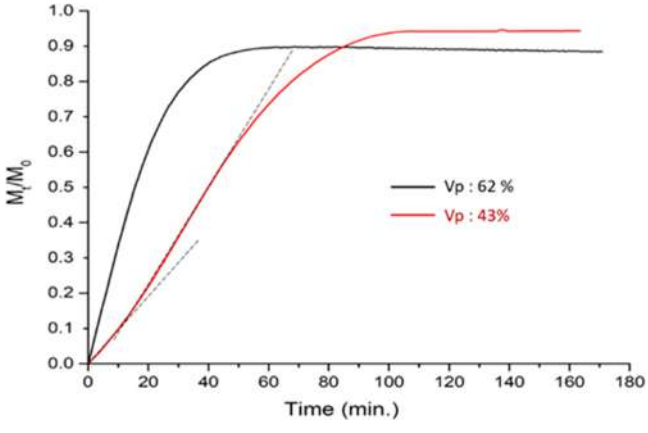

Figure 9. Dissolved silica mass M_t normalized on initial silica mass M_0 during dissolution in PBS at 37 °C for mesoporous silica films (CTAB templated, *Pm*3*n* structure) treated at 450 °C, before (black curve, sample CT450-3) and after (red curve, sample CT450-4) contamination from environmental VOC adsorbate. Porous volume is reduced from 62 to 43% and accessible surface area from 850 to 600 m^2 cm^{-3}. The red curve presents two different slopes at the beginning of dissolution and after 15 min shows an acceleration in the dissolution rate due to pore opening.

https://dx.doi.org/10.1021/acsami.9b19956
ACS Appl. Mater. Interfaces 2020, 12, 13598−13612

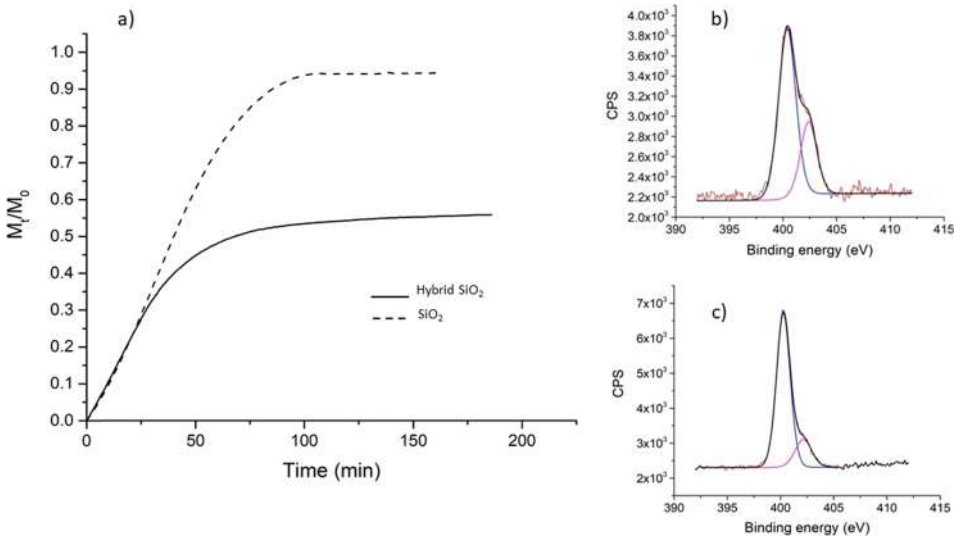

Figure 10. (a) Dissolution curve of mesoporous hybrid organosilica (solid line, sample NCT130-1) and silica (dashed line, sample CT130-3) in PBS at 37 °C. (b) XPS peak of nitrogen from hybrid organosilica sample before dissolution; we observe the peak of free amine (400 eV) and the peak of amine interacting with silanols (402.5 eV). (c) XPS peak of nitrogen from hybrid organosilica sample after 3 h of dissolution; the peak at 402.5 decreased.

water and a more open diffusive path. As a consequence, a pore-blocking effect must be investigated. To verify this hypothesis, we artificially blocked some pores of freshly made mesoporous samples by adsorption of preformed gold clusters. Mesoporous films were soaked 1 min in an ethanol-based solution containing 4-aminothiophenol stabilized gold NPs with size distribution ranging from 0.5 to 3.5 nm, and we obtained sigmoidal dissolution curves (data are reported in the Supporting Information), confirming that blocking some mesopores induces a decrease in the dissolution rate due to a reduction of accessible reactive surface and/or a hindered diffusion of silicate species. So, basically, we can consider adsorbed molecules or particles as a means to temporarily modify the accessible surface area of mesoporous materials, tuning their dissolution kinetics. This is a very interesting behavior for drug delivery applications because it means that (i) the dissolution kinetics of silica-based vectors is highly correlated with their drug loading and (ii) mesoporous particles hosting hydrophobic drugs will dissolve with a lag-time due to their cargo acting as a pore-blocking agent for water. Yet, if water can diffuse through the drug, intermediate effects can be expected. These results are in good accordance with previous works of drug release found for drug-templated silica materials.[45−48]

Globally, if one analyzes the kinetic sequence of a high-surface-area mesoporous silica carrier loaded with a poorly water-soluble drug, we see that it will consist of (i) a slow dissolution of the silica carrier before drug release (just after injection, for example), (ii) a progressive drug release (ideally at the target position), and (iii) concomitantly with drug release, an acceleration of the silica carrier dissolution. This is close to the ideal kinetic sequence envisioned at the beginning of this manuscript.

Dissolution of Amino-Functionalized Mesoporous Silica. In practical applications, silica is often employed as hybrid silica, containing organic functions such as methyl or amine anchored on the surface or in the silica matrix. Silica carrying amine moieties is particularly interesting for drug delivery applications because of its easy functionalization chemistry, which allows binding proteins, dyes, or antibodies to the surface.[49,50] Anyway, the presence of organic groups is known to decrease sensibly silica hydrolysis due to the inductive effect of alkyl chains, which gives electron density to the silicon centers.[7,49] Hydrophobic organic chains have an additional effect on silica dissolution by modifying the water hydrogen-bonding network close to the hybrid material surface, decreasing the affinity of water molecules for the surface.

We thus investigated the dissolution kinetics in physiological conditions of hybrid amino-functionalized silica, mesostructured from the CTAB template. Comparing silica and hybrid organosilica with similar porosity (0.42 vol fraction) and surface area (600−650 m^2 cm^{-3}), we noticed a very similar dissolution rate in the first 25 min, then the hybrid organosilica dissolution rate slowed down sensibly, and after 60 min of dissolution (50% of total mass released), the dissolution rate changed to a much slower one (Figure 10a) for the following 15 h. This behavior suggests a dissolution mechanism in two steps, where in a first time the hydrolysis concerns those Si−O bonds, which are far enough from the alkylammonium moieties, not to be influenced by the inductive effect of the organic group, and behave as if they belong to a pure silica structure. This is supported by the fact that the starting dissolution rate is coherent with the one of pure silica layers having the same characteristics. In a second step, the hybrid network dissolves, and the dissolution rate changes into a much slower one, in agreement with the kinetics previously reported for organosilica materials.[27,28,51,52] Besides, nucleophilic amino groups are excellent catalysts for silica hydrolysis, but this is not true for protonated aminosilanes. Thus, the starting rate of dissolution observed for hybrid organosilica could be due to a catalytic effect of nucleophilic amines, compensating the more hydrophobic nature of the material compared to silica. On the second part of the dissolution, inhibition due to both wetting and inductive effects could dominate, giving a slower dissolution rate. As a consequence, it is indeed very interesting to determine the number of nucleophilic amine moieties in the samples. For this reason,

https://dx.doi.org/10.1021/acsami.9b19956
ACS Appl. Mater. Interfaces 2020, 12, 13598−13612

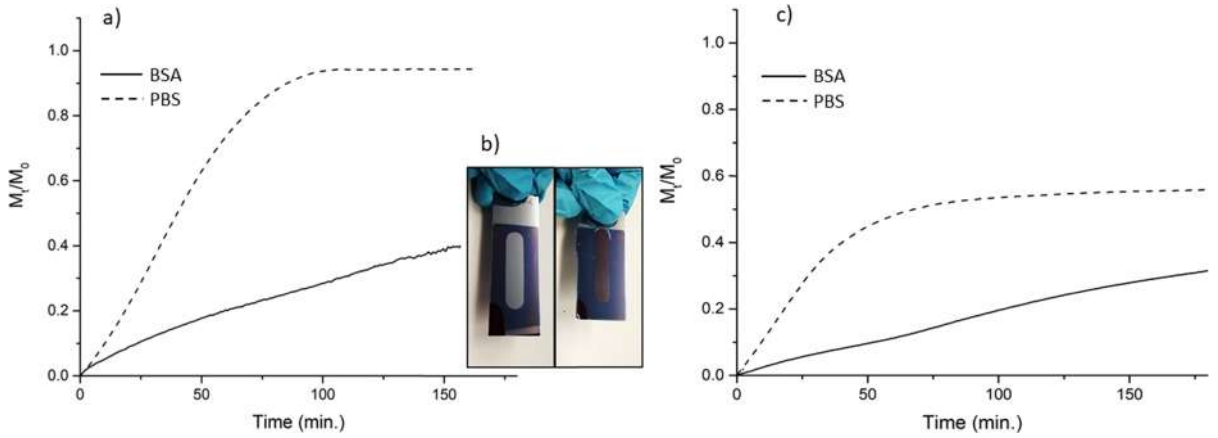

Figure 11. (a) Dissolution curves of mesoporous silica at 37 °C in PBS (dashed line, CT130-3) and in BSA solution (solid line, CT450-5). (b) Picture of mesoporous silica films after 3 h of dissolution in PBS (left) and BSA solution (right); after 3 h in PBS, there is no more silica left and the silicon substrate is visible, while after 3 h in BSA solution, a thick layer of silica is still present. (c) Dissolution curves of hybrid mesoporous organosilica at 37 °C in PBS (dashed line, NCT130-1) and in BSA solution (solid line, NCT130-2).

XPS analyses were performed on samples before and after 60 min of dissolution. The results confirmed our hypothesis, finding an increase in the N/Si ratio, which passes from 0.13 before dissolution to 0.38 after 60 min of dissolution (data calculated from survey spectra (reported in the Supporting Information, Figure S10)). Moreover, observing the nitrogen peak, we noticed a decrease in the peak at 402.5 eV, which is usually attributed to nucleophilic amines interacting through hydrogen bonding with silanols on the silica surface (Figure 10b,c). The peak decrease observed after dissolution can be due to reduced availability of silanols at the mesopore surface. As a conclusion, the slowing down of the dissolution rate after 60 min is likely to be due to a concomitant effect of amino-silane enrichment and progressive protonation of surface amines (inducing a progressive disappearance of nucleophilic centers able to catalyze silica hydrolysis). The contributions of the inductive effect, hydrophobic effect, and catalytic effect cannot be easily correlated at this point.

These results demonstrate that playing on the composition of hybrid organosilica makes possible to tune the dissolution kinetics easily. The influence of the structuring agent on the homogeneity of the dispersion of organic functions and thus on its dissolution behavior seems to be a crucial point since an excess in amine functions may destabilize the hybrid silica network, making in some cases the overall material less stable, as already observed.[7] More generally, the reported behavior is interesting for drug delivery applications because the amine group can interact with drugs loaded in the mesopores, retaining them and releasing them more slowly, while molecules bonded on the silica part could be released faster. Indeed, the behavior of drug-loaded hybrid nanoparticles will strongly depend on the matrix/drug interaction and on the solubility of the drug, but the two-step dissolution behavior observed for hybrid organosilica could be used to control drug release from mesoporous nanoparticles.

Degradation in Protein Solutions. Silica dissolution experiments in PBS allow relating some silica structural properties with its degradation kinetics. These data provide useful information that can be used for optimizing the material synthesis in order to modify its degradation rate in biological media. However, silica dissolution in biological environments is strongly influenced also by the dissolving media, which usually contains electrolytes and biomolecules. For example, it is nowadays established that a layer of proteins (corona) forms onto the surface of nanoparticles when they are in contact with biological fluids.[53−56] The protein corona mediates the interactions of nanomaterials with cells, and it determines nanoparticle biocompatibility and biodistribution.

To mimic biological environments more closely, we performed degradation experiments in a solution containing proteins with concentration comparable to the one present in the blood. We used 37.5 mg mL^{-1} BSA in PBS. In these conditions, BSA will be in its N form and will have a global negative surface charge.[57] Silica has also a negative surface charge at neutral pH, but protein adsorption takes place anyway,[58] mainly for entropic reasons, via hydrogen-bonding interactions between the silica surface silanols and the amino-acid chains of BSA. At such concentration, we assume a uniform adsorbed layer on the silica surface. In our degradation experiments (Figure 11), we observed that, at an early time (less than 50 min), the presence of proteins slowed down silica dissolution by a factor of 5. Moreover, a close look at Figure 11a showed that the initial dissolution rate decreases progressively in the first 60 min for reaching another slower regime. This observation is fully consistent with the time needed for the complete formation of a tighter BSA hard corona onto silica nanoparticles.[59,60]

Removing samples after 3 h of soaking at 37 °C and measuring them by ellipsometry after a quick rinsing with water, we found almost no silica residual layer (1−5 nm) for samples soaked in PBS, while samples soaked in BSA solution still presented a thick layer of silica (about 70% of the starting thickness), as shown in Figure 11b.

Silica dissolution happens at a slower rate in the presence of proteins, likely due to a barrier effect to diffusion caused by protein adsorption onto the surface, as already reported.[61] This barrier effect is likely to be due to the capping of mesopores. This behavior is consistent with the retarded drug release observed by Shahabi et al.[53] for porous silica nanoparticles in the presence of proteins. Hybrid organosilica presents also a similar behavior, with a consistent slowdown in the dissolution rate in protein-enriched media, as shown in Figure 11c, and a dissolution rate that decreases in the first 20 min until it reaches a constant rate. Qualitatively, the same effect of the protein surface layer on the dissolution rate has been observed for every sample analyzed, independent from its porosity,

https://dx.doi.org/10.1021/acsami.9b19956
ACS Appl. Mater. Interfaces 2020, 12, 13598−13612

structure, composition, and thermal treatment. This strengthens the hypothesis that the main effect of proteins is the hindrance to the diffusion process of dissolved species from the porous network to the bulk solution. The dissolution rate of the hybrid film is similar to that of pure silica film after 60 min, as evident from Figure 12. This suggests that the hard corona

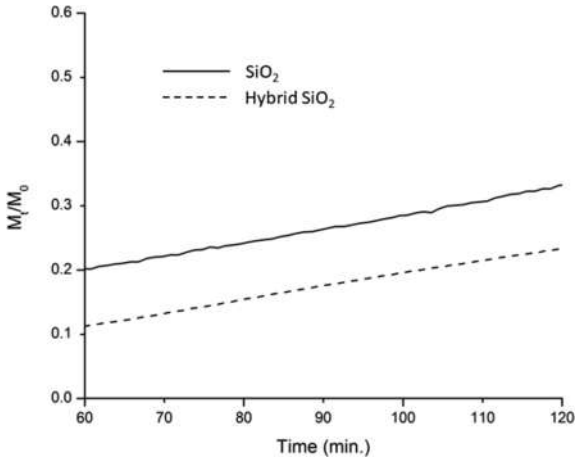

Figure 12. Blow up of dissolution curves of mesoporous silica (solid line) and hybrid organosilica (dashed line) at 37 °C in BSA solution, after the first 60 min.

of BSA is forming faster onto hybrid films than onto the silica film, probably due to the presence of the additional ammonium groups of the organosilica.

At that point, it is important to highlight that, if the protein corona controls particles' bioactivity, on the other hand, particles may have reverse effects on biomolecules that can be harmful. In fact, binding to nanoparticles can affect the structure and function of proteins (they can unfold and be denatured by the contact with the particle's surface, losing their function such as enzymatic activity), with catastrophic effects on cellular metabolism, and they can also undergo fibrillation due to the contact with nanomaterials.[62,63] The modification of the protein structure is one of the main mechanisms of toxicity associated with nanoparticles in vivo. Residual molecules from particle's synthesis can also react with proteins and denature them, causing damages to cellular metabolism. While we were performing silica dissolution experiments in protein solutions, we could observe sometimes an effect of the residual CTAB surfactant on surface adsorbed BSA (cf. Figure 13).

In fact, a large majority of mesostructured silica-based therapeutic vectors are prepared by using the CTAB surfactant. This CTAB is then removed by solvent extraction. In our samples whose surfactant was removed by thermal treatment at 450 °C, the refractive index of the mesoporous layer decreases as described here above during dissolution (Figure 13b). In solvent-extracted samples, the refractive index decrease is interrupted after 40 min of dissolution, and then its value starts increasing sensibly until it reaches the starting value in about 40 min. After 80 min, it decreases again constantly (Figure 13a).

In order to determine if this behavior comes from the presence of residual CTAB, we reabsorbed CTAB in the pores of a calcined clean sample (CT450) by soaking it in an ethanolic solution of CTAB and observed that its dissolution presents a similar transient "sinusoidal" evolution of refractive index value. This confirms the role of CTAB in the observed phenomenon. From the literature, we know that CTAB forms a protein-surfactant complex with BSA, not soluble in water, unfolding the protein and inducing its aggregation with other BSA molecules.[64,65] The positively charged head group of CTAB interacts electrostatically with carboxylic groups of aspartic acid and glutamic acid on BSA, which are deprotonated at pH = 7.4. This process reduces the ζ potential of BSA, triggering aggregation after an initial lag phase, which was found to last around 20 min.[64] The presence of this CTAB-BSA complex and/or the BSA aggregates on the surface of mesoporous silica films could explain the optical response of the washed mesoporous silica layers. Following the dissolution of the same films by surface plasmon resonance (SPR), we could observe a sudden decrease in the material refractive index when injecting the protein solution with the dissolution medium. This behavior was not observed in PBS, sustaining the hypothesis of a CTAB-BSA complex formation. In SPR experiments, we could flush both PBS and BSA solution on the same sample in two different channels and compare the two dynamics being sure that there was no difference due to material synthesis. In Figure 14a (washed film with remaining CTAB), BSA injection promotes a decrease of the SPR angle (related to the refractive index of the film), which goes below the value of the film maintained in PBS. This behavior can be explained with a decrease in the refractive index due to the diffusion of CTAB molecules outside the silica matrix. Later, the SPR angle increases, responding to a higher refractive index due to protein adsorption onto the film's surface. This is the expected behavior, which has been observed on dense silica

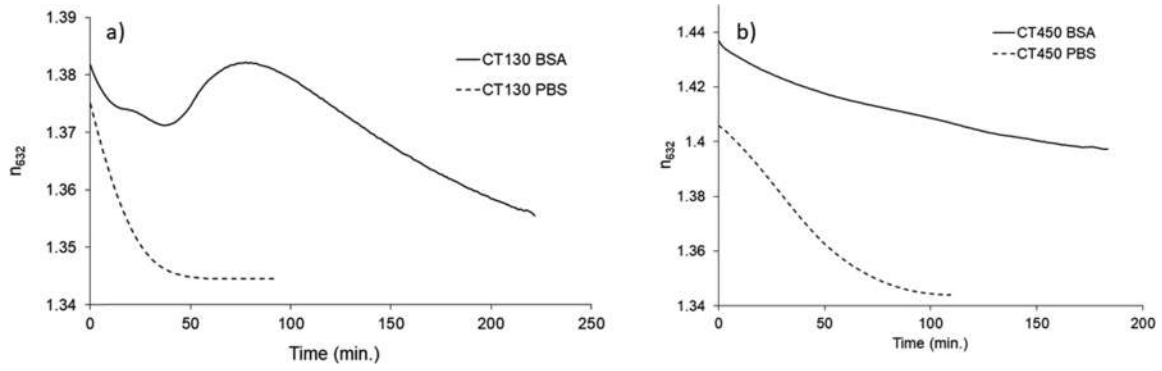

Figure 13. Refractive index at 632 nm of a mesoporous silica layer during dissolution in BSA solution at 37 °C for (a) the sample washed to remove CTAB and (b) the sample heated at 450 °C to remove CTAB.

https://dx.doi.org/10.1021/acsami.9b19956
ACS Appl. Mater. Interfaces 2020, 12, 13598−13612

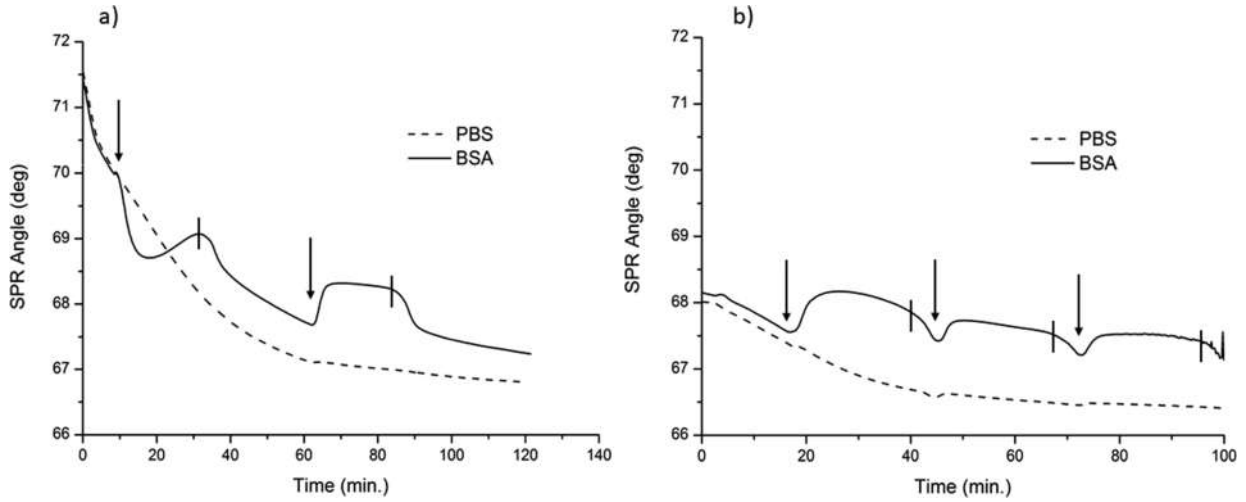

Figure 14. SPR angle shift of mesoporous silica layer (a) containing CTAB and (b) without CTAB. On the same sample were used parallel cells of 1 μL volume; in the first, PBS buffer was flushed, and in the second, PBS buffer and BSA solution were flushed alternatively. Arrows indicate the BSA solution injections, while the vertical lines indicate the buffer injections. The flow speed was 10 μL min^{-1}. In panel (b), the sample was washed with EtOH/HCl 100:1 (5 × 5 min), kept overnight in EtOH, and washed again (3 × 10min) before the dissolution experiment took place to be sure to extract all CTAB from the mesoporous film.

(not shown) as well as on films where CTAB was efficiently removed (Figure 14b).

By analyzing washed samples of silica films prepared with CTAB, we found that the residual amount of CTAB is very small because it was not possible to detect it by ellipsometry in air or by XPS, but it is enough to form some CTAB-BSA complex and adsorb it on the surface of the film. The amount of these aggregates is probably very low and does not seem to influence the overall dissolution kinetics (considering the residual silica after 3 h, measured ex situ), but it is enough to be detected by in situ ellipsometry because it modifies sensibly the optical response of the sample. More generally, the observation of this phenomenon points out how important is the washing step in the synthesis protocol of nanoparticles made for drug delivery. This effect may explain some discrepancies in the literature onto the colloidal stability of some silica-based therapeutic vectors dispersed in protein-rich media. As importantly, if the conformation of adsorbed protein may be not a major issue for dissolution experiments, it is indeed very important in a biological environment. The formation of protein-ligand complexes provokes the unfolding of the native structure of proteins and can be a starting point for aggregation, which compromises their biological function. It has been demonstrated in the case of CTAB in which the reduced ζ potential of the complex CTAB-BSA promotes aggregation.[64] Complexes with BSA have also been observed for other surfactants such as anionic sodium dodecyl sulfate (SDS) and nonionic polyoxyethylene-8-lauryl ether.[65] As therapeutic vectors usually cannot be calcined (nanoparticles can aggregate during thermal treatments, and they contain usually some organic ligands), solvent extraction is usually the chosen method to eliminate surfactants from nanocarriers. These results highlight how important it is to use a very optimized washing protocol for preparing nanoparticles allowing and ensuring the complete removal of the templating surfactant.

Finally, we did not observe the formation of CTAB-BSA complexes onto the surface of hybrid organosilica films, although they have been washed with ethanol to remove the surfactant with the same protocol used for pure silica films. We can infer that the washing was more efficient in the case of hybrid organosilica, probably because of the electrostatic repulsions between the cationic head of CTAB and the protonated amines on the silica surface. Nevertheless, hybrid silica materials carrying amine moieties have a modified surface charge compared to silica, depending on their aminosilane content. These materials can reach neutral to positive surface charges, depending on their synthesis conditions, strongly influencing adsorption and denaturation of biomolecules. We were not able to detect visible aggregation and denaturation due to surface charge on the hybrid organosilica films or the effect of the CTAB residual presence on BSA conformation. Anyway, the dissolution of silica and hybrid organosilica films in protein media could present some differences due to the altered surface charge of the two materials. For determining the exact effect of a moderate surface amine content on protein-surface interactions, a dedicated study would be necessary, which is not the objective of this work.

CONCLUSIONS

This study illustrates the set of chemical and physicochemical parameters that can be used to tune the degradation of therapeutic silica-based carriers in simulated biological media. In summary, the influence of several synthesis and structural parameters on mesoporous silica degradation was investigated by a standard and well-controlled in situ ellipsometry analysis platform. We demonstrated that the main factor controlling the silica dissolution rate is its accessible surface area (with a linear relationship) and that its mesostructure arrangement and thermal treatment have a minor impact on the overall kinetics. Anyway, a structure with high tortuosity can dissolve slower, as already evidenced by Braun et al.,[16] because the dissolution relies on molecular diffusion. The method employed in this work allowed us to split the process of silica dissolution into two parts: inside and outside the porous network. We found that, in the first phase, the concentration of dissolved silica reaching the external surface of the porous material depends linearly on the surface area. This result explains the key role of the surface area in the mesoporous silica degradation in

https://dx.doi.org/10.1021/acsami.9b19956
ACS Appl. Mater. Interfaces 2020, 12, 13598−13612

aqueous media, already identified by Kuroda et al.[46] and Shi et al.[9] Kuroda and co-workers demonstrated that silica particles with similar surface area have nearly identical degradability rates regardless of their diameter. On the other hand, Shi and co-workers[9] have studied the hydrolytic degradation of mesoporous silica with increasing surface area and found faster kinetics for higher surface areas. Moreover, we studied silica films having the same porous volume but different surface areas, separating the contributions of these two physicochemical parameters, which are often correlated, and we confirmed that the key feature controlling silica degradation in aqueous media is its surface area. We also observed that pore-blocking can introduce a lag-time in the dissolution kinetics, useful to tune drug carrier degradation and release. This effect is most probably due to a decrease in the available surface area caused by pore-blocking and/or an increase of tortuosity in the porous structure. The obtained results on the silica degradation rate were consistent with the ones reported by He et al.[9] for undersaturated media and comparable with data from Braun et al.,[16] considering differences in saturation conditions and surface evolution. Mesoporous silica films of 100−120 nm thickness dissolve completely in PBS at 37 °C within a few hours. We observed that hybrid organosilica mesostructured from CTAB and carrying propylamine moieties degrades in two steps and with an overall slower rate than pure silica. We verified that the observed kinetics are respected even in the case of films made of nanoparticles, meaning that degradation data obtained from thin films can be applied to predict NP behavior.

The degradation of mesoporous silica and hybrid organosilica in media containing high concentrations of proteins is slowed down. It was demonstrated that surface adsorbed molecules decrease the dissolution rate forming a barrier to diffusion.

Additionally, we demonstrated that residual surfactant molecules in the mesopores can influence the interactions of the material with biomolecules and reshape the interface, even if their amount is very low. They can unfold proteins forming stable complexes and induce protein aggregation, which can be harmful to cellular processes. This underlines the importance of efficient protocols to remove surfactants and other synthesis reagents from NPs employed for drug delivery purposes.

Considering the different physicochemical properties and degradation kinetics of each MSN system, researchers can select the best nanoplatform to fulfill a specific application. If long-term circulation times are needed, hybrid silica-containing organic functions or Zr-doped silica would be probably the best candidates because of their intrinsic higher hydrolytic stability. Hybrid organosilica can also be interesting to release drugs with two different kinetics due to its domain structure: a burst release in the first hours can be followed by a much slower release over several days. Whether the nanoparticles are used as imaging or delivery platforms for long-term applications, their surface area should be kept as low as possible without compromising their function. On the contrary, if a fast degradation is desired, the surface area should be high. For delivery carriers, it must be remembered than the loading of cargoes also tunes the nanoparticles degradation kinetics; thus, a cargo, which has strong interaction with the host matrix, can be capable to introduce a non-negligible lag-time in the degradation and in the drug release, providing good timing for targeted delivery without the need of gate blockers. One main issue when designing MSN as drug delivery platforms is to avoid their aggregation, remembering that surface functionalization stabilizes them also toward degradation, prolonging their lifetimes.

As a future perspective, we feel that it would be interesting to study mesoporous silica degradation behavior in dynamic conditions, in contact with flowing biological fluids, mimicking more closely the in vivo environment and addressing flow effects on silica dissolution.

■ ASSOCIATED CONTENT

Supporting Information

The Supporting Information is available free of charge at https://pubs.acs.org/doi/10.1021/acsami.9b19956.

Solution preparation procedures; GI-SAXS patterns of mesoporous films; environmental ellipsometric porosimetry (EEP) curves; derivation of silica dissolution from ellipsometry data; IR spectrum of VOC-contaminated mesoporous silica film; gold cluster synthesis and adsorption in mesopores of hybrid silica films: protocols, TEM, UV−vis spectrum, fluorescence spectrum; approximation of the erfc(x) function; XPS analysis of amino-functionalized mesoporous silica films before and after dissolution (PDF)

■ AUTHOR INFORMATION

Corresponding Author

Cédric Boissière − *Laboratoire Chimie de la Matière Condensée de Paris, UMR 7574, Sorbonne Université, 75252 Paris, France;* orcid.org/0000-0003-1212-6850; Email: cedric.boissiere@upmc.fr

Authors

Elisa Bindini − *Laboratoire Chimie de la Matière Condensée de Paris, UMR 7574, Sorbonne Université, 75252 Paris, France; Centre de Nanosciences et de Nanotechnologies (C2N), CNRS, 91120 Palaiseau, France*

Zeinab Chehadi − *Laboratoire Chimie de la Matière Condensée de Paris, UMR 7574, Sorbonne Université, 75252 Paris, France*

Marco Faustini − *Laboratoire Chimie de la Matière Condensée de Paris, UMR 7574, Sorbonne Université, 75252 Paris, France;* orcid.org/0000-0002-6254-5116

Pierre-Antoine Albouy − *Laboratoire de Physique des Solides, UMR 8502, Université Paris Sud, 510 Orsay, France;* orcid.org/0000-0002-5350-2042

David Grosso − *Institut Matériaux Microélectronique Nanoscience de Provence, 13397 Marseille, France;* orcid.org/0000-0002-9156-6848

Andrea Cattoni − *Centre de Nanosciences et de Nanotechnologies (C2N), CNRS, 91120 Palaiseau, France*

Corinne Chanéac − *Laboratoire Chimie de la Matière Condensée de Paris, UMR 7574, Sorbonne Université, 75252 Paris, France*

Omar Azzaroni − *Instituto de Investigaciones Fisicoquímicas Teóricas y Aplicadas, B1900 La Plata, Argentina;* orcid.org/0000-0002-5098-0612

Clément Sanchez − *Laboratoire Chimie de la Matière Condensée de Paris, UMR 7574, Sorbonne Université, 75252 Paris, France;* orcid.org/0000-0002-6426-4844

Complete contact information is available at: https://pubs.acs.org/10.1021/acsami.9b19956

https://dx.doi.org/10.1021/acsami.9b19956
ACS Appl. Mater. Interfaces 2020, 12, 13598−13612

Author Contributions

The manuscript was written through contributions of all authors. All authors have given approval to the final version of the manuscript.

Notes

The authors declare no competing financial interest.

■ ACKNOWLEDGMENTS

C.B. received funding from the region Ile de France AFA2014_INTERBIODYN. C.S. received funding from College de France.

■ REFERENCES

(1) Lin, Y.-S.; Hurley, K.; Haynes, C. L. Critical Considerations in the Biomedical Use of Mesoporous Silica Nanoparticles. *J. Phys. Chem. Lett.* **2012**, 364−374.
(2) Argyo, C.; Weiss, V.; Bräuchle, C.; Bein, T. Multifunctional Mesoporous Silica Nanoparticles as a Universal Platform for Drug Delivery. *Chem. Mater.* **2014**, *26*, 435−451.
(3) Kim, J.; Lee, J. E.; Lee, J.; Jang, Y.; Kim, S.-W.; An, K.; Yu, J.; Hyeon, T. Generalized Fabrication of Multifunctional Nanoparticle Assemblies on Silica Spheres. *Angew. Chem., Int. Ed.* **2006**, *45*, 4789−4793.
(4) Bao, G.; Mitragotri, S.; Tong, S. Multifunctional Nanoparticles for Drug Delivery and Molecular Imaging. *Annu. Rev. Biomed. Eng.* **2013**, *15*, 253−282.
(5) Warren, S. C.; DiSalvo, F. J.; Wiesner, U. Nanoparticle-tuned Assembly and Disassembly of Mesostructured Silica Hybrids. *Nat. Mater.* **2007**, *6*, 156−161.
(6) Mulvaney, P.; Liz-Marzán, L. M.; Giersig, M.; Ung, T. Silica Encapsulation of Quantum Dots and Metal Clusters. *J. Mater. Chem.* **2000**, *10*, 1259−1270.
(7) Fontecave, T.; Sanchez, C.; Azaïs, T.; Boissière, C. Chemical Modification As a Versatile Tool for Tuning Stability of Silica Based Mesoporous Carriers in Biologically Relevant Conditions. *Chem. Mater.* **2012**, *24*, 4326−4336.
(8) Mortera, R.; Fiorilli, S.; Garrone, E.; Verné, E.; Onida, B. Pores Occlusion in MCM-41 Spheres Immersed in SBF and the Effect on Ibuprofen Delivery Kinetics: A Quantitative Model. *Chem. Eng. J.* **2010**, *156*, 184−192.
(9) He, Q.; Shi, J.; Zhu, M.; Chen, Y.; Chen, F. The Three-Stage In Vitro Degradation Behavior of Mesoporous Silica in Simulated Body Fluid. *Microporous Mesoporous Mater.* **2010**, *131*, 314−320.
(10) Bass, J. D.; Grosso, D.; Boissiere, C.; Belamie, E.; Coradin, T.; Sanchez, C. Stability of Mesoporous Oxide and Mixed Metal Oxide Materials under Biologically Relevant Conditions. *Chem. Mater.* **2007**, *19*, 4349−4356.
(11) Li, X.; Barua, S.; Rege, K.; Vogt, B. D. Tuning Stability of Mesoporous Silica Films under Biologically Relevant Conditions through Processing with Supercritical CO_2. *Langmuir* **2008**, *24*, 11935−11941.
(12) Lin, Y.-S.; Abadeer, N.; Haynes, C. L. Stability of Small Mesoporous Silica Nanoparticles in Biological Media. *Chem. Commun.* **2011**, *47*, 532−534.
(13) Cauda, V.; Schlossbauer, A.; Bein, T. Bio-Degradation Study of Colloidal Mesoporous Silica Nanoparticles: Effect of Surface Functionalization with Organo-Silanes and Poly(ethylene glycol). *Microporous Mesoporous Mater.* **2010**, *132*, 60−71.
(14) Quignard, S.; Mosser, G.; Boissière, M.; Coradin, T. Long-Term Fate of Silica Nanoparticles Interacting With Human Dermal Fibroblasts. *Biomaterials* **2012**, *33*, 4431−4442.
(15) Yu, T.; Malugin, A.; Ghandehari, H. Impact of Silica Nanoparticle Design on Cellular Toxicity and Hemolytic Activity. *ACS Nano* **2011**, *5*, 5717−5728.
(16) Braun, K.; Pochert, A.; Beck, M.; Fiedler, R.; Gruber, J.; Lindén, M. Dissolution Kinetics of Mesoporous Silica Nanoparticles in Different Simulated Body Fluids. *J. Sol-Gel Sci. Technol.* **2016**, *79*, 319−327.
(17) Andersson, J.; Rosenholm, J.; Areva, S.; Lindén, M. Influences of Material Characteristics on Ibuprofen Drug Loading and Release Profiles from Ordered Micro- and Mesoporous Silica Matrices. *Chem. Mater.* **2004**, *16*, 4160−4167.
(18) Izquierdo-Barba, I.; Colilla, M.; Manzano, M.; Vallet-Regí, M. In vitro Stability of SBA-15 Under Physiological Conditions. *Microporous Mesoporous Mater.* **2010**, *132*, 442−452.
(19) Feliu, N.; Docter, D.; Heine, M.; del Pino, P.; Ashraf, S.; Kolosnjaj-Tabi, J.; Macchiarini, P.; Nielsen, P.; Alloyeau, D.; Gazeau, F.; Stauber, R.; Parak, W. In vivo Degeneration and the Fate of Inorganic Nanoparticles. *Chem. Soc. Rev.* **2016**, *45*, 2440−2457.
(20) Icenhower, J. P.; Dove, P. M. The Dissolution Kinetics of Amorphous Silica into Sodium Chloride Solutions: Effects of Temperature and Ionic Strength. *Geochim. Cosmochim. Acta* **2000**, *64*, 4193−4203.
(21) Cauda, V.; Argyo, C.; Bein, T. Impact of Different PEGylation Patterns on the Long-term Bio-stability of Colloidal Mesoporous Silica Nanoparticles. *J. Mater. Chem.* **2010**, *20*, 8693−8699.
(22) Zhang, H.; Dunphy, D. R.; Jiang, X.; Meng, H.; Sun, B.; Tarn, D.; Xue, M.; Wang, X.; Lin, S.; Ji, Z.; Li, R.; Garcia, F.; Yang, J.; Kirk, M.; Xia, T.; Zink, J.; Nel, A.; Brinker, C. Processing Pathway Dependence of Amorphous Silica Nanoparticle Toxicity: Colloidal vs Pyrolytic. *J. Am. Chem. Soc.* **2012**, *134*, 15790−15804.
(23) Dove, P.; Han, N.; Wallace, A.; De Yoreo, J. Kinetics of Amorphous Silica Dissolution and the Paradox of the Silica Polymorphs. *Proc. Natl. Acad. Sci.* **2008**, *105*, 9903−9908.
(24) Alexander, G. B.; Heston, W. M.; Iler, R. K. The Solubility of Amorphous Silica in Water. *J. Phys. Chem.* **1954**, *58*, 453−455.
(25) Fournier, R. O.; Rowe, J. J. The Solubility of Amorphous Silica in Water at High Temperatures and High Pressures. *Am. Mineral.* **1977**, *62*, 1052−1056.
(26) Tompkins, H.; Irene, E. Eds., *Handbook of Ellipsometry*; William Andrew Pub. ; Springer: Norwich, NY : Heidelberg, Germany, 2005.
(27) Urata, C.; Yamada, H.; Wakabayashi, R.; Aoyama, Y.; Hirosawa, S.; Arai, S.; Takeoka, S.; Yamauchi, Y.; Kuroda, K. Aqueous Colloidal Mesoporous Nanoparticles with Ethenylene-Bridged Silsesquioxane Frameworks. *J. Am. Chem. Soc.* **2011**, *133*, 8102−8105.
(28) Datz, S.; Engelke, H.; Schirnding, C. V.; Nguyen, L.; Bein, T. Lipid Bilayer-Coated Curcumin-based Mesoporous Organosilica Nanoparticles for Cellular Delivery. *Microporous Mesoporous Mater.* **2016**, *225*, 371−377.
(29) Grosso, D.; Cagnol, F.; Soler-Illia, G. D. A.; Crepaldi, E. L.; Amenitsch, H.; Brunet-Bruneau, A.; Bourgeois, A.; Sanchez, C. Fundamentals of Mesostructuring Through Evaporation-Induced Self-Assembly. *Adv. Funct. Mater.* **2004**, *14*, 309−322.
(30) Boissiere, C.; Grosso, D.; Lepoutre, S.; Nicole, L.; Bruneau, A. B.; Sanchez, C. Porosity and Mechanical Properties of Mesoporous Thin Films Assessed by Environmental Ellipsometric Porosimetry. *Langmuir* **2005**, *21*, 12362−12371.
(31) Löbmann, P. Characterization of Sol−Gel Thin Films by Ellipsometric Porosimetry. *J. Sol-Gel Sci. Technol.* **2017**, *84*, 2−15.
(32) Grosso, D.; Babonneau, F.; Albouy, P.-A.; Amenitsch, H.; Balkenende, A.; Brunet-Bruneau, A.; Rivory, J. An in Situ Study of Mesostructured CTAB−Silica Film Formation during Dip Coating Using Time-Resolved SAXS and Interferometry Measurements. *Chem. Mater.* **2002**, *14*, 931−939.
(33) Noyes, A. A.; Whitney, W. R. The Rate of Solution of Solid Substances In Their Own Solutions. *J. Am. Chem. Soc.* **1897**, *19*, 930−934.
(34) Levich, V. *Physicochemical Hydrodynamics*; Prentice-Hall, 1962.
(35) Nernst, W. Theorie der Reaktionsgeschwindigkeit in Heterogenen Systemen. *Z. Für Phys. Chem.* **1904**, *47U*, 52−55.
(36) Brunner, E. Reaktionsgeschwindigkeit in Heterogenen Systemen. *Z. Für Phys. Chem.* **1904**, *47U*, 56−102.
(37) Hixson, A.; Crowell, J. Dependence of Reaction Velocity upon surface and Agitation. *Ind. Eng. Chem.* **1931**, *23*, 923−931.

https://dx.doi.org/10.1021/acsami.9b19956
ACS Appl. Mater. Interfaces 2020, 12, 13598−13612

(38) Rebiscoul, D.; Frugier, P.; Gin, S.; Ayral, A. Protective Properties and Dissolution Ability of the Gel Formed During Nuclear Glass Alteration. *J. Nucl. Mater.* **2005**, *342*, 26−34.
(39) Frugier, P.; Gin, S.; Minet, Y.; Chave, T.; Bonin, B.; Godon, N.; Lartigue, J.-E.; Jollivet, P.; Ayral, A.; De Windt, L.; Santarini, G. SON68 Nuclear Glass Dissolution Kinetics: Current State of Knowledge and Basis of the New GRAAL Model. *J. Nucl. Mater.* **2008**, *380*, 8−21.
(40) Geisler, T.; Dohmen, L.; Lenting, C.; Fritzsche, M. Real-time In Situ Observations of Reaction and Transport Phenomena During Silicate Glass Corrosion by Fluid-cell Raman Spectroscopy. *Nat. Mater.* **2019**, *18*, 342.
(41) Bunker, B. C.; Tallant, D. R.; Headley, T. J.; Turner, G. L.; Kirkpatrick, R. J. The Structure of Leached Sodium Borosilicate Glass. *Phys. Chem. Glasses* **1988**, *29*, 106−120.
(42) Hellmann, R.; Eggleston, C. M.; Hochella, M. F., Jr.; Crerar, D. A. The Formation of Leached Layers on Albite Surfaces During Dissolution Under Hydrothermal Conditions. *Geochim. Cosmochim. Acta* **1990**, *54*, 1267−1281.
(43) Higuchi, T. Mechanism of Sustained-Action Medication. Theoretical Analysis of Rate of Release of Solid Drugs Dispersed in Solid Matrices. *J. Pharm. Sci.* **1963**, *52*, 1145−1149.
(44) Irwin, A. D.; Holmgren, J. S.; Jonas, J. Solid-state 29Si NMR Study of Polycondensation During Heat Treatment of Sol-Gel-Derived Silicas. *Mater. Lett.* **1987**, *6*, 25−30.
(45) Huang, X.; Young, N. P.; Townley, H. E. Characterization and Comparison of Mesoporous Silica Particles for Optimized Drug Delivery. *Nanomater. Nanotechnol.* **2014**, *4*, 2.
(46) Yamada, H.; Urata, C.; Aoyama, Y.; Osada, S.; Yamauchi, Y.; Kuroda, K. Preparation of Colloidal Mesoporous Silica Nanoparticles with Different Diameters and Their Unique Degradation Behavior in Static Aqueous Systems. *Chem. Mater.* **2012**, *24*, 1462−1471.
(47) Croissant, J. G.; Fatieiev, Y.; Khashab, N. M. Degradability and Clearance of Silicon, Organosilica, Silsesquioxane, Silica Mixed Oxide, and Mesoporous Silica Nanoparticles. *Adv. Mater.* **2017**, *29*, 1604634.
(48) Fontecave, T.; Boissiere, C.; Baccile, N.; Plou, F. J.; Sanchez, C. Using Evaporation-Induced Self-Assembly for the Direct Drug Templating of Therapeutic Vectors with High Loading Fractions, Tunable Drug Release, and Controlled Degradation. *Chem. Mater.* **2013**, *25*, 4671−4678.
(49) Hoffmann, F.; Cornelius, M.; Morell, J.; Fröba, M. Silica-Based Mesoporous Organic−Inorganic Hybrid Materials. *Angew. Chem. Int. Ed.* **2006**, *45*, 3216−3251.
(50) Liberman, A.; Mendez, N.; Trogler, W. C.; Kummel, A. C. Synthesis and Surface Functionalization of Silica Nanoparticles for Nanomedicine. *Surf. Sci. Rep.* **2014**, *69*, 132−158.
(51) Koike, N.; Ikuno, T.; Okubo, T.; Shimojima, A. Synthesis of Monodisperse Organosilica Nanoparticles with Hollow Interiors and Porous Shells Using Silica Nanospheres as Templates. *Chem. Commun.* **2013**, *49*, 4998−5000.
(52) Croissant, J. G.; Cattoën, X.; Man, M. C. W.; Durand, J.-O.; Khashab, N. M. Syntheses and Applications of Periodic Mesoporous Organosilica Nanoparticles. *Nanoscale* **2015**, *7*, 20318−20334.
(53) Shahabi, S.; Döscher, S.; Bollhorst, T.; Treccani, L.; Maas, M.; Dringen, R.; Rezwan, K. Enhancing Cellular Uptake and Doxorubicin Delivery of Mesoporous Silica Nanoparticles via Surface Functionalization: Effects of Serum. *ACS Appl. Mater. Interfaces* **2015**, *7*, 26880−26891.
(54) Fleischer, C. C.; Payne, C. K. Nanoparticle−Cell Interactions: Molecular Structure of the Protein Corona and Cellular Outcomes. *Acc. Chem. Res.* **2014**, *47*, 2651−2659.
(55) Walkey, C. D.; Olsen, J. B.; Guo, H.; Emili, A.; Chan, W. C. Nanoparticle Size and Surface Chemistry Determine Serum Protein Adsorption and Macrophage Uptake. *J. Am. Chem. Soc.* **2012**, *134*, 2139−2147.
(56) Lundqvist, M.; Augustsson, C.; Lilja, M.; Lundkvist, K.; Dahlbäck, B.; Linse, S.; Cedervall, T. The Nanoparticle Protein Corona Formed in Human Blood or Human Blood Fractions. *PLoS One* **2017**, *12*, No. e0175871.
(57) Givens, B. E.; Xu, Z.; Fiegel, J.; Grassian, V. H. Bovine Serum Albumin Adsorption on SiO2 and TiO2 Nanoparticle Surfaces at Circumneutral and Acidic pH: A Tale of Two Nano-bio Surface Interactions. *J. Colloid Interface Sci.* **2017**, *493*, 334−341.
(58) Qiu, Y.; Liu, Y.; Wang, L.; Xu, L.; Bai, R.; Ji, Y.; Wu, X.; Zhao, Y.; Li, Y.; Chen, C. Surface Chemistry and Aspect Ratio Mediated Cellular Uptake of Au Nanorods. *Biomaterials* **2010**, *31*, 7606−7619.
(59) Monopoli, M. P.; Walczyk, D.; Campbell, A.; Elia, G.; Lynch, I.; Baldelli Bombelli, F.; Dawson, K. A. Physical−Chemical Aspects of Protein Corona: Relevance to in Vitro and in Vivo Biological Impacts of Nanoparticles. *J. Am. Chem. Soc.* **2011**, *133*, 2525−2534.
(60) Orts-Gil, G.; Natte, K.; Thiermann, R.; Girod, M.; Rades, S.; Kalbe, H.; Thünemann, A.; Maskos, M.; Österle, W. On the Role of Surface Composition and Curvature on Biointerface Formation and Colloidal Stability of Nanoparticles in a Protein-rich Model System. *Colloids Surf., B* **2013**, *108*, 110−119.
(61) Yang, S.-A.; Choi, S.; Jeon, S.; Yu, J. Silica Nanoparticle Stability in Biological Media Revisited. *Sci. Rep.* **2018**, *8*, 185.
(62) Vertegel, A.; Siegel, R.; Dordick, J. Silica Nanoparticle Size Influences the Structure and Enzymatic Activity of Adsorbed Lysozyme. *Langmuir* **2004**, *20*, 6800−6807.
(63) Rodriguez, C. E.; Fukuto, J. M.; Taguchi, K.; Froines, J.; Cho, A. K. The Interactions of 9,10-phenanthrenequinone with Glyceraldehyde-3-phosphate Dehydrogenase (GAPDH), a Potential Site for Toxic Actions. *Chem.-Biol. Interact.* **2005**, *155*, 97−110.
(64) Sharma, A.; Agarwal, P. K.; Deep, S. Characterization of Different Conformations of Bovine Serum Albumin and Their Propensity to Aggregate in the Presence of N-cetyl-N,N,N-trimethyl Ammonium Bromide. *J. Colloid Interface Sci.* **2010**, *343*, 454−462.
(65) Valstar, A.; Almgren, M.; Brown, W.; Vasilescu, M. The Interaction of Bovine Serum Albumin with Surfactants Studied by Light Scattering. *Langmuir* **2000**, *16*, 922−927.

https://dx.doi.org/10.1021/acsami.9b19956
ACS Appl. Mater. Interfaces 2020, 12, 13598−13612